Chinese Chemical Letters 32 (2021) 1442–1446

Contents lists available at ScienceDirect

Chinese Chemical Letters

journal homepage: www.elsevier.com/locate/cclet

Communication

Three-dimensional porous photo-thermal fiber felt with salt-resistant property for high efficient solar distillation

Jingjing Zhang[a,1], Xueqing Luo[a,1], Xiaoxin Zhang[a], Ying Xu[d], Hongbo Xu[b], Jinlong Zuo[c,*], Dongmei Liu[a,*], Fuyi Cui[a], Wei Wang[a,*]

[a] State Key Laboratory of Urban Water Resource and Environment, School of Environment, Harbin Institute of Technology, Harbin 150090, China
[b] School of Chemistry and Chemical Engineering, Harbin Institute of Technology, Harbin 150090, China
[c] Department of Environmental Engineering, Harbin University of Commerce, Harbin 150076, China
[d] School of Ecology and Environment, Zhengzhou University, Zhengzhou 450000, China

ARTICLE INFO

Article history:
Received 24 July 2020
Received in revised form 4 September 2020
Accepted 6 October 2020
Available online 7 October 2020

Keywords:
Solar distillation
Photo-thermal evaporation
Solar desalination
Salt resistance
Solar evaporation

ABSTRACT

The urgent need for fresh water resource is a public issue facing the world. Solar distillation for seawater desalination is a promising freshwater production method. Interfacial solar evaporation systems based on 2D photo-thermal membranes have been widely studied, but salt pollution is one of the main challenges for solar distillation. In order to solve this problem, a hydrophilic three-dimensional (3D) porous photo-thermal fiber felt (PFF) was obtained by one-step method, through a simple polydopamine (PDA) coating method with hydrophobic graphite felt as a substrate. The PFF had a good evaporation rate of 1.48 kg m^{-2} h^{-1} and its corresponding light-vapor conversion efficiency reached 87.4%. In addition, the PFF exhibited an excellent salt-resistant ability when applied to photo-thermal evaporation of high-salinity seawater with 10 wt% NaCl, owing to its intrinsic 3D macroporous structure for the migration circulation of salt ions. The development of the PFF offers a new route for the exploration of salt-resistant photo-thermal materials and is promising for the practical application of solar distillation.

The lack of freshwater resource is a livelihood crisis facing the world. Apart from traditional water purification methods (physical and chemical methods, biological methods, *etc.*), new sustainable methods need to be developed to increase freshwater supply [1–6]. In recent years, solar distillation has received more and more attention in the field of seawater desalination, benefiting from the sufficient seawater content and an abundant supply of solar energy on earth [7–9]. Solar desalination technology has undergone natural evaporation, nano-fluid-based solar heating and interfacial solar heating [10–12]. The former two utilize solar energy to heat the entire liquid directly or indirectly, resulting in lower evaporation rates and energy conversion efficiencies. Based on the principle that evaporation is essentially interfacial activity, interfacial solar heating technology has been vigorously studied by researchers. The integrated evaporation system of the photo-thermal material and the thermal insulation component achieves an effective management of thermal energy while ensuring the sufficient light absorption of the light absorbent [13–15]. Among them, solar desalination based on two-dimensional (2D) photo-thermal membranes as light absorbers has been widely developed.

2D photo-thermal membranes with high light absorption have been extensively explored in the past decade, including plasmonic metals based on plasmon resonance, semiconductors featuring electron-hole generation and relaxation and carbonaceous materials deriving from the photo-thermal mechanism of thermal vibration of molecules [16–21]. In general, the application of photo-thermal membrane for solar evaporation mainly relies on a porous hydrophilic substrate as a carrier, thus could simultaneously achieve light absorption and water transportation [22,23]. Otherwise, for photo-thermal materials that are inherently hydrophobic, the light-to-vapor conversion efficiency would remain at a lower level due to the obstacle of water transportation [24–26]. However, the 2D photo-thermal membranes used in solar desalination are now facing the severe problem of salt deposition. Several studies that have been reported demonstrated the occurrence of salt deposition on the photo-thermal membranes for seawater (3.5 wt% NaCl) desalination under solar illumination [27–29]. The occurrence of salt deposition should be mainly

* Corresponding authors.
E-mail addresses: mdjzjl@163.com (J. Zuo), mei18@hit.edu.cn (D. Liu), wangweirs@hit.edu.cn, psweiwang@aliyun.com (W. Wang).
[1] These authors contributed equally to this work.

https://doi.org/10.1016/j.cclet.2020.10.004
1001-8417/

because that the rate of upward transport and surface deposition of salt ions on the 2D membrane during solar-driven desalination process is greater than the release rate of salt ions into the bulk solution. The problem of membrane fouling caused by salt deposition is a serious challenge to the durability of the photo-thermal materials. Hence, it is urgent to develop more photo-thermal materials with salt-resistant property for the practical application requirements of future photo-thermal desalination. Recently, the researches of 3D porous photo-thermal materials for solar desalination have been developed to a certain extent, mainly focusing on carbon aerogels, porous biomass-derived carbon materials, graphene foams, *etc.* [19,30–32]. Additionally, several 3D photo-thermal evaporators for salt-water separation during solar desalination were also explored [33,34]. The preparation methods or processes of most of the reported 3D photo-thermal materials were relatively harsh (high temperature or high pressure) or complicated (Multi-step processing *etc.*).

In this work, a hydrophilic 3D porous photo-thermal fiber felt (PFF) was obtained by one-step method, through a simple and facile interfacial polymerization of polydopamine (PDA) on a common hydrophobic graphite felt [35,36]. Graphite fiber felt itself has an excellent light absorption property, while PDA with good light absorption capacity also plays an important wetting role here to promote water transport capacity of the PFF. In addition, the PFF achieved an outstanding photo-thermal evaporation rate of 1.48 $kg\,m^{-2}\,h^{-1}$ and its associated evaporation efficiency reached 87.4%. More importantly, the PFF has an excellent resistance to salt pollution under high salt concentration condition (10 wt% NaCl). The internal 3D structure of the PFF provides sufficient transport channels for the salt ions migration cycle compared to traditional 2D photo-thermal membranes (Fig. 1). The simple preparation and excellent reusability of the PFF provides a bright prospect for the practical industrial application of solar desalination.

The morphologies of the 3D porous graphite felt (GF) before and after modification were examined by scanning electron microscope (SEM). By observing the microstructure of pristine GF shown in Fig. 2a, it could be seen that GF was composed of multi-layer fibers with the average diameter of about 8 μm. Furthermore, the sufficient porosity and channels of the GF would facilitate the transport of water and water vapor. However, the water contact angle (WCA) of $130 \pm 5°$ in the inset displayed that the pristine GF had poor wettability, which would be adverse to the application of hydrophobic GF on solar evaporation. As shown in Fig. 2b, plentiful PDA particles could be clearly observed on the graphite fibers of the PFF and its pore structure was maintained well simultaneously. The WCA of the PFF was tested to be 0°, indicating that the hydrophilicity of the PFF was significantly improved by the modification of PDA. Furthermore, the corresponding energy dispersive spectrometer (EDS) mapping images of PFF fibers clearly demonstrated the evenly distribution of C, N and O, indicating the existence of PDA (Figs. 2c–f). The photographs of PFF before and after 1 h ultrasonic treatment were listed in Fig. S1 (Supporting information), and the aqueous solution with little change after ultrasound could preliminarily show the stability of PDA loaded on the PFF fibers. In addition, the chemical composition of the hydrophilic PFF was examined by X-ray photoelectron spectroscopy (XPS) (Fig. 2g). As expected, the three dominating peaks were C—O bonding (286.3 eV), C—N bonding (285.8 eV) and C—C bonding (284.6 eV), respectively, which laterally demonstrated that the hydrophilic PFF contained a certain amount of PDA. Raman spectra showed that the ratios of I_D/I_G of the PFF and GF were 1.03 and 0.93, respectively (Fig. 2h). It illustrated that the introduction of PDA increased the defect ratio of GF, and further enhanced the hydrophilic properties of the PFF. The light absorption capacities of GF before and after modification were compared by full spectral absorption. As is shown in Fig. 2i, both GF and PFF had superior light absorption performance in the full spectral region with an average light absorbance of more than 90%. Moreover, it could be found that the existence of PDA particles promoted the improvement of the light absorption performance of the PFF.

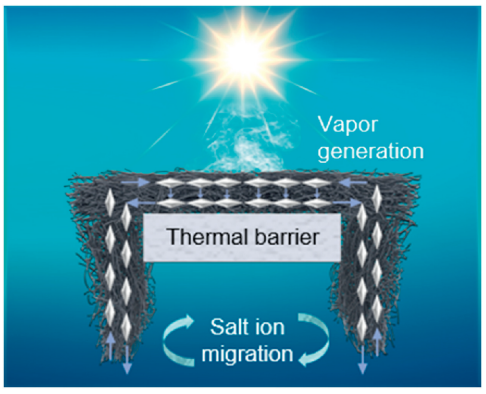

Fig. 1. Schematic illustration of solar desalination based on PFF.

To evaluate the solar evaporation capacity of the PFF, the evaporation system was constructed. As shown in Fig. 3a, under irradiation of a solar simulator, the PFF supported by a piece of insulation foam was installed at the center of a beaker and its edges were immersed in pure water. Additionally, the solar evaporation of the GF was also examined in the case of GF floating directly on water. As recorded in Fig. 3b, we measured the mass change of the evaporation system to compare the evaporation performance of the PFF and GF. In the absence of photo-thermal material, the evaporation rate of pure water was only 0.42 $kg\,m^{-2}\,h^{-1}$ due to the low light absorption capacity of water. The evaporation rate of 1.00 $kg\,m^{-2}\,h^{-1}$ of GF should result from its hydrophobicity and the substantial heat loss of its evaporation system. Obviously, the PFF had optimal solar evaporation performance with the evaporation rate of 1.48 $kg\,m^{-2}\,h^{-1}$, resulting from its remarkable solar energy absorption, superior hydrophilicity and little heat loss. As revealed in Fig. S2 (Supporting information), the solar vapor conversion efficiency of the system also confirmed that the PFF had a significant advantage in solar evaporation. The efficiency of the PFF was calculated to be 87.4%, which was far greater than that of GF (47.0%) and pure water (8.1%). Furthermore, the evaporation performances of the PFF for pure water and salt solution of NaCl (with the mass fraction of 3.5 wt% NaCl) were investigated under different solar power densities, respectively. As shown in Fig. 3c, there was no significant difference in the evaporation rates for pure water and 3.5 wt% NaCl solution under identical irradiation, indicating that the existence of 3.5 wt% NaCl in the solution hardly affected the evaporation effect of the system. More remarkably, the evaporation rates of the two solutions grew linearly as the solar power density increased. Besides, the surface temperatures of the evaporation system among different solar illumination were measured by IR camera (Fig. S3 in Supporting information). To be specific, the maximum surface temperature of the PFF rose from 42.5 °C under 1 sun (1 kW/m^2 solar irradiation) to 50.2 °C under 2 sun. As light density further increased, the maximum surface temperature reached 57.0 °C under 3 sun and 63.9 °C under 4 sun. It is shown from the results that the variation of the maximum temperature in the adjacent groups was similar, which was consistent with the linear enhancement of the solar evaporation of the PFF with the increase of irradiation.

The influence of different NaCl concentrations for evaporation performances of the PFF was further investigated. It could be observed from Fig. 4a that the water mass loss of NaCl solutions with a mass fraction less than 7% remained basically unchanged

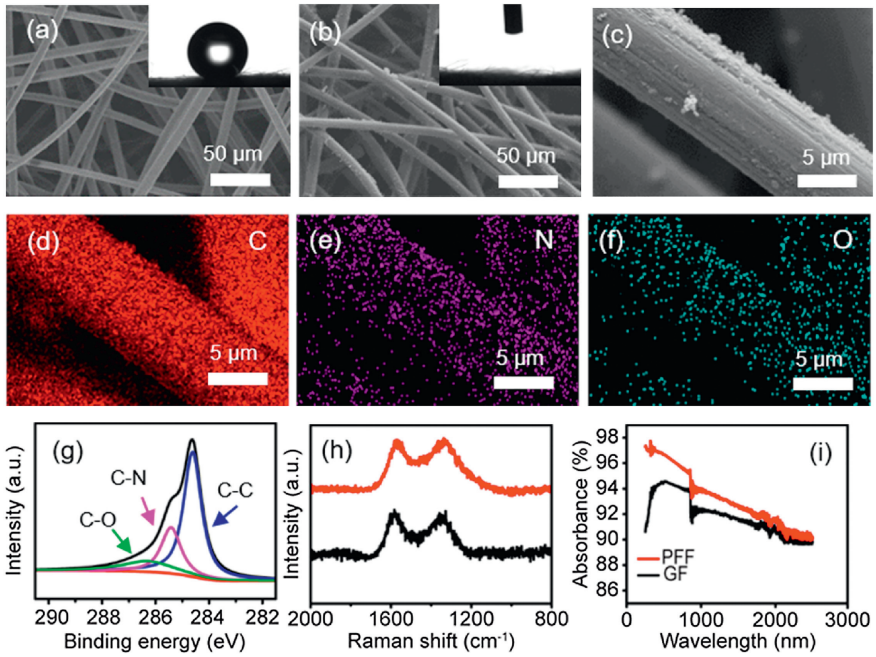

Fig. 2. SEM images of (a) pristine GF and (b) PFF, the insets are the corresponding water contact angles. (c) High-magnification SEM image of the PFF single fiber. (d-f) EDS mapping images of C, N and O elements. (g) XPS spectra of PFF. (h) Raman spectra comparison of PFF and GF. (i) Full spectra absorption of GF and PFF.

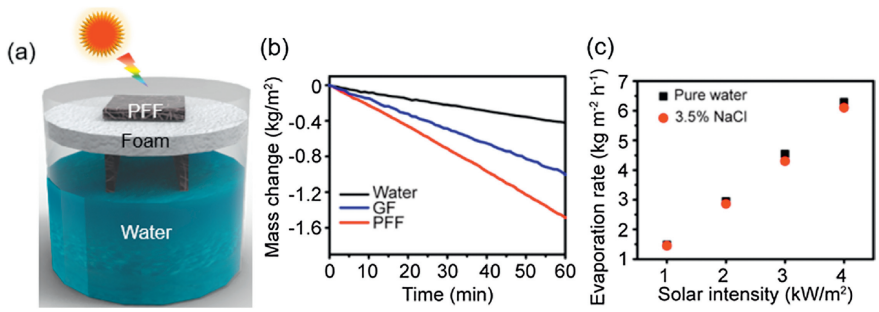

Fig. 3. (a) Schematic of the solar evaporation system based on PFF. (b) Water mass change with time under 1 sun irradiation for different photo-thermal materials. (c) Solar evaporation rates of PFF under different solar intensities.

with increased salt concentration, which was about 11.51 kg/m^2 after 8 h of solar illumination. For 10 wt% NaCl solution, the water mass loss reduced to 10.25 kg/m^2. The little decrease of the evaporation rate for high concentration salt solution could be due to the increase of the hydration force between salt ions and water molecules. In addition, the surface changes appeared on the PFF were recorded throughout the evaporation process of different NaCl solutions (Fig. 4b and Fig. S4 in Supporting information). Although the solution salinity reached up to 10 wt%, it could be found that no salt crystal was observed on the PFF surface after 8 h of solar illumination. From the SEM image of PFF after evaporation (Fig. 4c), only a few NaCl crystals were deposited on the PFF fibers. However, the porous channels were not blocked due to the existence of large-sized pores and the internal 3D structure of the PFF. The small residual NaCl deposited on the fibers could be totally removed by repeated water cleaning.

The salinity of the evaporation system was shown in Fig. 4d, the salt concentration of the treated brine was a little higher than the original salinity, and the relatively low salinity of the PFF evaporation surface also showed the existence of salt on the PFF structure. The salt concentration approaching zero further confirmed that the slight salt particles could be completely eliminated by simple cleaning. The above results exhibited the outstanding salt-resistant capacity of the 3D porous PFF. In addition, the evaporation performance of the GF aimed at 10 wt % NaCl was tested to be much poorer than that of the PFF (Fig. S5 in Supporting information). The total water mass loss of the evaporation system after 8 h illumination was measured to be 7.39 kg/m^2, even though the GF surface did not yet have salt crystallization due to its hydrophobic nature. Hydrophobic photo-thermal materials rely on their surface hydrophobicity to localize solar heat and promote water evaporation. Nevertheless, their evaporation performance is far less than that of hydrophilic materials equipped with heat insulation devices. To interpret the salt-rejecting mechanism of the PFF, the migration path of salt ions was illustrated in Fig. 4e. The PFF as 3D porous fiber felt could provide sufficient inner structure for the migration circulation of salt ions between the interior of the fiber felt and the salt solution filled in the beaker. Almost all of the salt ions were recycled to the residual solution of the beaker within the evaporation process, which insured the salt-resistant function of the PFF. Contrastively, the occurrence of salt accumulation for the common 2D photo-thermal membranes should be due to the lack of space, thus caused the blocking of the migration circulation of salt ions (Fig. S6 in Supporting information). The evaporation performances of PFF for two weeks' use proved almost unchanged (Fig. 4f). The surface

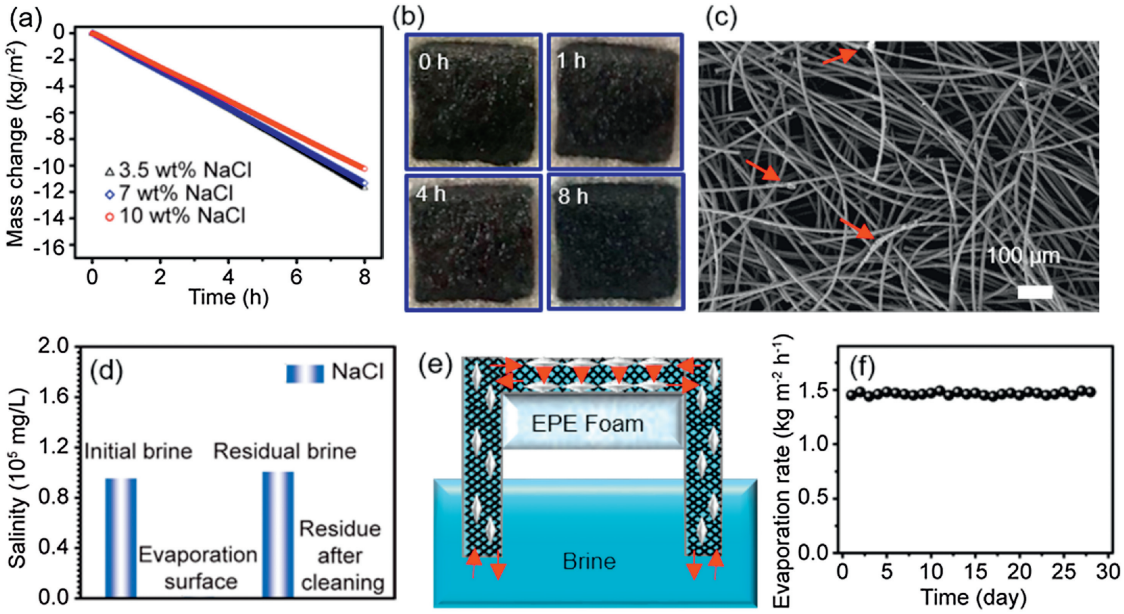

Fig. 4. (a) Mass change of the evaporation system with time for different NaCl concentration under 1 kW/m^2 solar illumination. (b) Photographs of salt deposition (10 wt% NaCl) on PFF within 8 h illumination. (c) Surface morphology of PFF after solar evaporation of 10 wt% NaCl. (d) Comparison of salt content of the evaporation system before and after evaporation. (e) Schematic illustration of salt ions migration circulation of the evaporation system based on PFF. (f) Long-term evaporation performance test of PFF with 10 wt% NaCl.

morphology of PFF (Fig. S7 in Supporting information) indicated the stability of PDA on the PFF during solar desalination.

To explore the impurities removal ability of the PFF, the water quality before and after evaporation were further analyzed. Taking the actual seawater (South China Sea, China) as a raw water source, we tested the elements content in the initial seawater and the distilled water by ICP-OES. As revealed in Fig. 5a, the salinities of five dominating inorganic salt ions (Na^+, K^+, Ca^{2+}, Mg^{2+} and B^{3+}) in the initial seawater dropped several orders of magnitude after distillation, indicating the effective desalination capacity of the PFF. In addition, the distillation effect of heavy metallic solution with Cu^{2+}, Cd^{2+}, Ni^{2+} and Zn^{2+} as four targets was investigated, and the concentration of the four heavy metal ions in raw water comparatively dropped by more than 98% after evaporation (Fig. 5b). Except for the inorganic salts, organic matters were also considered as common contaminant. Hence, the dye solutions of methylene blue, methyl orange and rhodamine B with the same concentration of 100 mg/L were selected to examine the organic matter removal ability of the PFF. As shown in Fig. S8 (Supporting information), the UV–vis spectrum demonstrated the PFF equally possessed the broad prospect for the organics removal in solar distillation.

In conclusion, the 3D porous PFF was successfully fabricated for solar distillation. Thanks to the excellent photo-thermal property and wetting property of the PFF, it achieved good light-vapor conversion. More significantly, the fiber felt displayed outstanding salt resistance when applied to photo-thermal evaporation of high-salinity seawater, which benefited from its intrinsic 3D structure. In addition, the PFF also showed superior performance in the desalination treatment of actual seawater and simulated heavy metal wastewater. This study could open up new paths for the salt-resistant photo-thermal materials and promote the practical industrial application of solar distillation.

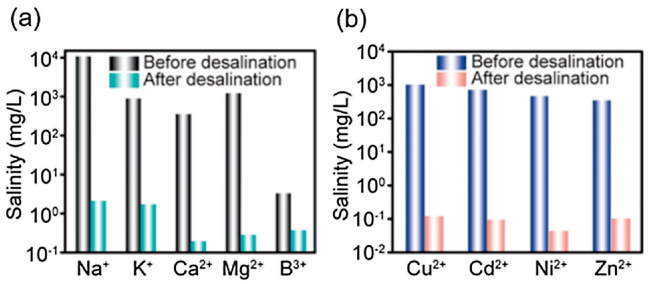

Fig. 5. Salinity comparison of (a) actual seawater and (b) simulated heavy metal wastewater before and after solar desalination based on PFF.

Declaration of competing interest

The authors report no declarations of interest.

Acknowledgments

The authors gratefully acknowledge the National Natural Science Foundation of China (No. 52070052), Natural Science Foundation of Heilongjiang Province (No. YQ2020B003), the State Key Laboratory of Urban Water Resource and Environment (HIT, No 2021TS03), and National Science and Technology Major Project (No. 2017ZX07501002).

Appendix A. Supplementary data

Supplementary material related to this article can be found, in the online version, at doi:https://doi.org/10.1016/j.cclet.2020.10.004.

References

[1] C. Walden, W. Zhang, Environ. Sci. Technol. 50 (2016) 8417–8431.
[2] A.K. Ghattas, F. Fischer, A. Wick, T.A. Ternes, Water Res. 116 (2017) 268–295.
[3] W. Zhong, Y. Zhang, L. Zhao, W. Li, Chin. Chem. Lett. 31 (2020) 2651-2656.
[4] Z. Zhu, Y. Liu, H. Hou, et al., Environ. Sci. Technol. 52 (2018) 3027–3036.
[5] X. Wang, Y. Pan, H. Yuan, et al., Chin. Chem. Lett. 31 (2020) 365–368.
[6] G. Ni, G. Li, S.V. Boriskina, et al., Nat. Energy 1 (2016) 16126.
[7] M. Elimelech, W.A. Phillip, Science 333 (2011) 712–717.
[8] M. Gao, L. Zhu, C.K. Peh, G.W. Ho, Energy Environ. Sci. 12 (2019) 841–864.
[9] Z. Li, C. Wang, Chin. Chem. Lett. 31 (2020) 2159-2166.
[10] A.H. Cavusoglu, X. Chen, P. Gentine, O. Sahin, Nat. Commun. 8 (2017) 617.
[11] X. Wang, Y. He, X. Liu, L. Shi, J. Zhu, Sol. Energy 157 (2017) 35–46.

[12] Z. Wang, Y. Liu, P. Tao, et al., Small 10 (2014) 3234–3239.
[13] P. Tao, G. Ni, C. Song, et al., Nat. Energy 3 (2018) 1031–1041.
[14] W. Xu, X. Hu, S. Zhuang, et al., Adv. Energy Mater. 8 (2018) 1702884.
[15] G. Ni, S.H. Zandavi, S.M. Javid, et al., Energy Environ. Sci. 11 (2018) 1510–1519.
[16] M. Gao, P.K.N. Connor, G.W. Ho, Energy Environ. Sci. 9 (2016) 3151–3160.
[17] K. Bae, G. Kang, S.K. Cho, et al., Nat. Commun. 6 (2015) 10103.
[18] T. Murakami, H. Nakatsuji, M. Inada, et al., J. Am. Chem. Soc. 134 (2012) 17862–17865.
[19] M.W. Higgins, A. Shakeel Rahmaan, R.R. Devarapalli, M.V. Shelke, N. Jha, Sol. Energy 159 (2018) 800–810.
[20] X. Liu, X. Wang, J. Huang, G. Cheng, Y. He, Appl. Energy 220 (2018) 302–312.
[21] H. Wang, R. Wu, S. Wei, Chin. Chem. Lett. 27 (2016) 1572–1576.
[22] Z. Wang, Q. Ye, X. Liang, et al., J. Mater. Chem. A 5 (2017) 16359–16368.
[23] Y. Xu, H. Xu, Z. Zhu, et al., J. Mater. Chem. A 7 (2019) 22296–22306.
[24] L. Zhang, B. Tang, J. Wu, R. Li, P. Wang, Adv. Mater. 27 (2015) 4889–4894.
[25] Y. Xu, J. Ma, D. Liu, et al., Chem. Eng. J. 356 (2019) 869–876.
[26] Y. Zeng, J. Yao, B.A. Horri, et al., Energy Environ. Sci. 4 (2011) 4074–4078.
[27] C. Finnerty, L. Zhang, D.L. Sedlak, K.L. Nelson, B. Mi, Environ. Sci. Technol. 51 (2017) 11701–11709.
[28] Z. Liu, H. Song, D. Ji, et al., Glob. Challenges 1 (2017) 160003.
[29] Y. Jin, J. Chang, Y. Shi, et al., J. Mater. Chem. A 6 (2018) 7942–7949.
[30] Y. Gu, X. Mu, P. Wang, et al., Nano Energy 74 (2020) 104857.
[31] L. Li, T. Hu, A. Li, J. Zhang, ACS Appl. Mater. Interfaces 12 (2020) 32143–32153.
[32] W. Zhang, W. Zhu, S. Shi, et al., J. Mater. Chem. A 6 (2018) 16220–16227.
[33] L. Wu, Z. Dong, Z. Cai, et al., Nat. Commun. 11 (2020) 521.
[34] Y. Shi, C. Zhang, R. Li, et al., Environ. Sci. Technol. 52 (2018) 11822–11830.
[35] X. Wu, Q. Jiang, D. Ghim, S. Singamaneni, J. Mater. Chem. A 6 (2018) 18799–18807.
[36] X. Zeng, M. Luo, G. Liu, et al., Adv. Sci. 5 (2018) 1800510.